Approximate optimal LEO transfers with J2 perturbation and dragsail

(Article begins on next page)

28 April 2024

Approximate Optimal LEO Transfers with J2 Perturbation and Dragsail

Lorenzo Casalino[a,*], Andrea Forestieri[a]

[a]*Politecnico di Torino, Department of Mechanical and Aerospace Engineering, Corso Duca degli Abruzzi, 24, Torino, 10129, Italy*

Abstract

An indirect optimization method is applied to orbit transfers in LEO, considering almost circular orbits and the influence of J2 perturbation. An approach based on Edelbaum's approximation is employed to solve transfers with change of semimajor axis, inclination and right ascension of ascending node. The spacecraft employs electric propulsion either alone or in combination with a drag sail that can be deployed and retracted. The proposed formulation is simple and effective and is capable of treating both minimum-time (thruster is always on) and minimum-propellant (coasting arcs are introduced) problems, while also dealing with the presence of altitude constraints. Convergence to the optimal solution is fast and straightforward, making the proposed approach suitable for the preliminary evaluation of large sets of available transfers (e.g., multiple debris removal).

Keywords: Indirect optimization methods, Edelbaum approximation, Electric propulsion, Drag sail, J2 perturbation

1. Introduction

Satellite operations in low Earth orbit (LEO) are growing at a steady pace and transfers between LEOs will become increasingly frequent in the next future. Many missions, such as active debris removal, satellite refurbishing and maintenance, operations of small platforms, will require a spacecraft to maneuver between LEOs. Electric propulsion (EP) offers significant benefits in terms of propellant consumption and may be the preferred option for this kind of missions. The analysis and optimization of low-thrust EP trajectories in LEO is intrinsically complex. The transfers typically require a large number of revolutions around the Earth, with short and long period variations of the optimal controls. Increased complexity comes from the presence of perturbations, which

---
[*]Corresponding author

Email addresses: `lorenzo.casalino@polito.it` (Lorenzo Casalino), `andrea.forestieri@polito.it` (Andrea Forestieri)

make the two-body problem approximation not suited to deal with this kind of transfers.

Different techniques have been used to deal with this problem, both considering impulsive thrust or low-thrust (that is, EP): indirect approaches based on averaging techniques [1], global search algorithms [2] in conjunction with a surrogate model for the problem dynamics [3, 4, 5], particle swarm optimization [6], direct multiple shooting [7], pseudospectral methods [8]. Typically, these works search for a rather accurate optimization of the transfers, which is usually a demanding task from a computational point of view; in alternative, simplified formulas are used [9, 10], which may not deal with all the complexities of the solutions. A method for a quick but accurate estimation of transfer costs, in terms of time and propellant consumption, would obviously be very useful, and its development is the purpose of the present article.

Low Earth orbits have an altitude below 2000 km and therefore are characterized by low eccentricity (below 0.25). Most of the operational orbits have eccentricity values below 0.1 and the approximation of almost-circular orbits yields sufficiently accurate results. Edelbaum [11] used a building block approach to solve the minimum-time problem for unperturbed low-thrust transfers between circular inclined orbits. He first solved the one-revolution transfer to determine the optimal controls for changes of semimajor axis and inclination. He then used these results to determine the optimal multiple-revolution transfer that achieves the required changes of the two relevant orbital elements. The initial orbit plane is conveniently selected as the reference plane, and the other orbital elements (in particular, the right ascension of the ascending node, RAAN) can be ignored.

In LEO, the perturbation that comes from Earth's ellipsoidal shape has the most relevant effect, at least for those orbits that have sufficient altitude to remain stable for long times and suffer little aerodynamic effects. Earth's oblateness is accounted for by the Earth's gravitational harmonic J2 coefficient, which causes secular and short-period variations of the orbital elements. The inclusion of J2 effect is mandatory to obtain useful results in the analysis of transfers in LEO, except in the case of very short durations. In many cases of practical interest, such as, active debris removal, satellite refurbishing missions or operation of small-sat moving to and from the ISS, transfer preliminary analysis and optimization usually consider only the secular effects of J2 and neglect aerodynamic effects . In addition to the classical zero-drag model with secular J2-effect, aerodynamic drag is also considered here. The motivation of adding drag to the model was to analyze trajectories that exploit a retractable drag sail. Dragsails [12, 13, 14] are a promising technology for satellite deorbit and could profitably be exploited also for orbit transfers in LEO. Drag on a small spacecraft without sail is instead very small and minimally affects the results at the altitudes considered in this article.

Edelbaum's equation for almost-circular orbits have been in the past reconsidered to include perturbations and, namely, J2, in the analysis. Kechichian [15] introduced Earth oblateness in the equations for the equinoctial elements, and later derived an indirect approach to solve transfers between circular orbits

[16]. A similar technique was also used in a recent paper [17], but active change of the RAAN was not considered. Formulas to approximate the transfer ΔV as a function of change in semimajor axis, inclination and RAAN (taking the J2 perturbation into account) have also been proposed [9] and verified by means of an exact indirect optimization of the transfer with a homotopic approach. In the present article, the approach of Ref. [16] is revisited and extended to deal with low-thrust transfer between (almost) circular orbits, with secular perturbations of the orbital elements due to J2 and the presence of aerodynamic drag. In particular, a new control variable to seek an optimal change of the RAAN is introduced, minimum-propellant trajectories are considered alongside minimum-time transfers, altitude constraints are introduced, the effect of drag is added, and the control law for the sail area is determined.

The optimization problem requires finding the thrust direction to achieve rendezvous with a target spacecraft either in minimum time or with minimum propellant expenditure (given the trip time). The target orbit is here assumed to be only perturbed by J2, whereas the aerodynamic drag is neglected (or assumed to be somehow compensated). Since the orbits are almost circular, changes of eccentricity and argument of periapsis are not considered. Long missions with many revolutions are expected and proper phasing to rendezvous with the target can be achieved with minimal changes to the control program; for this reason, also the true anomaly equation is neglected. In the general problem, the chaser spacecraft is on an initial orbit specified by semimajor axis, inclination and RAAN at the initial time $t_0 = 0$. The target orbit is characterized by its own values of semimajor axis, inclination and RAAN (also specified at time $t_0 = 0$). The target RAAN changes with time, thus the required change depends on the trip time, which may be unknown.

This paper aims at finding an approximation of the optimal transfer between two perturbed LEO objects in terms of orbital changes to accomplish the maneuver with minimum propellant consumption or minimum time. An indirect method is first used to solve the optimal one-revolution transfer in the absence of aerodynamic drag (Sec. 2). These results lead to the formulation of differential equations for the orbital elements during the transfer, and indirect approach is used to define the optimal control laws (Sec. 3). The transfer optimization problem is defined and solved in Sec. 4. Section 5 considers the presence of aerodynamic drag and discusses the optimal use of a deployable/retractable sail. The procedure to solve the boundary value problem and find suitable initial guesses is described in Sec. 6. Test cases and results are presented in Sec. 7.

2. One-Revolution Transfer

The spacecraft is subject to the two-body problem equations perturbed by J2 and low-thrust acceleration. Aerodynamic drag is presently neglected and will be treated in Sec. 5. As already mentioned, almost circular orbits and long transfers are considered, and equations for eccentricity, argument of periapsis,

and mean anomaly are neglected. For low eccentricity ($e \approx 0$), radius, semimajor axis and semilatus rectum can be considered to be equal ($r \approx a \approx p$), and the velocity always coincides with the circular value ($V^2 \approx \mu/r$); μ is Earth's gravitational parameter. The harmonic coefficient J2 produces small short-period variations of the orbital elements which are neglected in the approximation adopted here. Only secular variation are accounted for, and, in particular for RAAN Ω, the time derivative is expressed as [18]

$$\dot{\Omega}_{J2} = -(3/2)J_2(r_E/a)^2(V/r)\cos\imath = -(3/2)J_2(r_E/a)^2\mu^{1/2}a^{-3/2}\cos\imath \qquad (1)$$

and only depends on orbit semimajor axis a (i.e., radius) and inclination $\imath$; r_E is Earth's radius.

Gauss' form of Lagrange's planetary equations [18, 19, 20] is used. The differential equations of the orbital elements are given as functions of orthogonal components of the perturbing acceleration, in this case, the thrust-to-mass ratio T/m. The radial acceleration component is zero when eccentricity is not changed [11] and the out-of-plane thrust angle is the only control variable for this problem. The secular perturbation $\dot{\Omega}_{J2}$ due to Earth's oblateness is added to evaluate the RAAN rate of change. The time differential equations for semimajor axis, inclination and RAAN are

$$\frac{\mathrm{d}a}{\mathrm{d}t} = 2\frac{a}{V}\frac{T}{m}\cos\beta \qquad (2)$$

$$\frac{\mathrm{d}\imath}{\mathrm{d}t} = \frac{1}{V}\frac{T}{m}\cos\vartheta\sin\beta \qquad (3)$$

$$\sin\imath\frac{\mathrm{d}\Omega}{\mathrm{d}t} = \frac{T}{m}\sin\vartheta\sin\beta - J_2\frac{3}{2}\left(\frac{r_E}{a}\right)^2\frac{V}{a}\cos\imath\sin\imath \qquad (4)$$

where the angle between thrust and orbit plane β has been introduced. These equations are rewritten using the longitude along the orbit ϑ (measured starting from the ascending node) as the independent variable, replacing time.

$$\frac{\mathrm{d}a}{\mathrm{d}\vartheta} = 2a\frac{T/m}{\mu/a^2}\cos\beta \qquad (5)$$

$$\frac{\mathrm{d}\imath}{\mathrm{d}\vartheta} = \frac{T/m}{\mu/a^2}\cos\vartheta\sin\beta \qquad (6)$$

$$\frac{\mathrm{d}\Omega}{\mathrm{d}\vartheta} = \frac{T/m}{\mu/a^2}\frac{\sin\vartheta}{\sin\imath}\sin\beta - J_2\frac{3}{2}\left(\frac{r_E}{a}\right)^2\cos\imath \qquad (7)$$

with the additional time equation

$$\frac{\mathrm{d}t}{\mathrm{d}\vartheta} = \sqrt{a^3/\mu} \qquad (8)$$

Both thrust and J2 perturbation are small, so semimajor axis, inclination and thrust acceleration can be treated as constant in the right-hand side of these equations.

The theory of optimal control [21, 22] is applied to determine the optimal control law. The Hamiltonian is defined by associating an adjoint variable λ to each differential equation

$$H = \lambda_a 2Aa\cos\beta + \lambda_\imath A\cos\vartheta\sin\beta + \lambda_\Omega\left[A\frac{\sin\vartheta}{\sin\imath}\sin\beta - J_2\frac{3}{2}\left(\frac{r_E}{a}\right)^2\cos\imath\right] \tag{9}$$

where the nondimensional acceleration $A = (T/m)/(\mu/a^2)$ has been introduced. Euler-Lagrange equations [21] state that the adjoint variables λ are actually adjoint constants, since H does not depend on the state variables in the one-revolution problem (as already stated, small orbital changes imply that a and $\imath$ can be treated as constant in the Hamiltonian).

The optimal thrust angle β is obtained by nullifying the partial derivative of H

$$\tan\beta = \frac{\lambda_\imath\cos\vartheta + (\lambda_\Omega/\sin i)\sin\vartheta}{2\lambda_a a} \tag{10}$$

It is important to note that the generic form of the optimal control as a function of state and adjoint variable does not formally depend on the actual performance index which is maximized and on the specific boundary conditions of the problem. One can introduce the angle ϑ_0

$$\tan\vartheta_0 = \frac{\lambda_\Omega/\sin\imath}{\lambda_\imath} \tag{11}$$

and the quantity $\Lambda = \sqrt{\lambda_\imath^2 + (\lambda_\Omega/\sin i)^2}$ to rewrite

$$\lambda_\imath = \Lambda\cos\vartheta_0 \qquad\qquad \lambda_\Omega/\sin i = \Lambda\sin\vartheta_0 \tag{12}$$

The optimal thrust angle is easily written as

$$\tan\beta = \frac{\Lambda}{2a\lambda_a}\cos(\vartheta - \vartheta_0) = K\cos(\vartheta - \vartheta_0) \tag{13}$$

The additional variable $\vartheta' = \vartheta - \vartheta_0$ is introduced and the thrust angle is defined by

$$\cos\beta = 1/K' \qquad\qquad \sin\beta = K\cos\vartheta'/K' \tag{14}$$

with $K' = \sqrt{1 + (K\cos\vartheta')^2}$. The differential equations finally become

$$\frac{da}{d\vartheta'} = A\frac{2r}{K'} \tag{15}$$

$$\frac{d\imath}{d\vartheta'} = A\frac{K\cos\vartheta'\cos(\vartheta' + \vartheta_0)}{K'} \tag{16}$$

$$\frac{d\Omega}{d\vartheta'} = \frac{A}{\sin\imath}\frac{K\cos\vartheta'\sin(\vartheta' + \vartheta_0)}{K'} - J_2\frac{3}{2}\left(\frac{r_E}{a}\right)^2\cos\imath \tag{17}$$

Integration over one revolution has a solution with elliptic integrals. When $\vartheta_0 = 0$ and J2 is neglected, these equations are the same as in Edelbaum's

5

problem [11] for changes in a and $\imath$. If the corresponding changes are indicated as Δa_0 and $\Delta \imath_0$ one can easily prove that

$$\Delta \imath = \Delta \imath_0 \cos \vartheta_0 \qquad\qquad \Delta \Omega = (\Delta \imath_0 / \sin \imath) \sin \vartheta_0 - 3\pi J_2 (r_e / a)^2 \cos \imath \quad (18)$$

Therefore, the angle ϑ_0 allows one to split the effect of out-of-plane thrusting between inclination and RAAN change.

Edelbaum showed that, when constant β with a sign switch every half revolution (at $\vartheta = \vartheta_0 + \pi/2 + k\pi$ for any integer k) is used instead of the optimal varying angle from Eq. (13), the performance decrease is minimal, and this suboptimal law is adopted here. With constant β, the equations of motions become analytically integrable. Subsequent integration along two half-revolutions, e.g., from $\vartheta_0 - \pi/2$ to $\vartheta_0 + \pi/2$ and then from $\vartheta_0 + \pi/2$ to $\vartheta_0 + 3\pi/2$ readily provides the changes over a complete revolution:

$$\Delta a \;=\; 4\pi \frac{T}{m} \frac{a^3}{\mu} \cos \beta \tag{19}$$

$$\Delta \imath \;=\; 4 \frac{T}{m} \frac{a^2}{\mu} \sin \beta \cos \vartheta_0 \tag{20}$$

$$\Delta \Omega \;=\; 4 \frac{T}{m} \frac{a^2}{\mu} \frac{\sin \beta}{\sin \imath} \sin \vartheta_0 - 3\pi J_2 \left(\frac{r_E}{a} \right)^2 \cos \imath \tag{21}$$

$$\Delta t \;=\; 2\pi \sqrt{\frac{a^3}{\mu}} \tag{22}$$

3. Multiple-Revolution Transfer

The differential equations to describe the multiple-revolution transfer are based on the previous analysis. The orbital elements changes which are obtained with constant-beta during one revolution are divided by the time needed for its completion to approximate the time derivatives of the orbital elements. The spacecraft mass is also added to the state equations, as mass consumption cannot in general be neglected for multiple-revolution transfers. One has

$$\frac{\mathrm{d}a}{\mathrm{d}t} \;=\; 2 \frac{T}{m} \sqrt{\frac{a^3}{\mu}} \cos \beta \tag{23}$$

$$\frac{\mathrm{d}\imath}{\mathrm{d}t} \;=\; \frac{2}{\pi} \frac{T}{m} \sqrt{\frac{a}{\mu}} \sin \beta \cos \vartheta_0 \tag{24}$$

$$\frac{\mathrm{d}\Omega}{\mathrm{d}t} \;=\; \frac{2}{\pi} \frac{T}{m} \sqrt{\frac{a}{\mu}} \sin \beta (\sin \vartheta_0 / \sin \imath) - J_2 \frac{3}{2} \left(\frac{r_E}{a} \right)^2 \sqrt{\frac{\mu}{a^3}} \cos \imath \tag{25}$$

$$\frac{\mathrm{d}m}{\mathrm{d}t} \;=\; -\frac{T}{c} \tag{26}$$

where $c = g_0 I_{sp}$ is the effective exhaust velocity, considered to be constant in the present analysis, g_0 is the gravitational acceleration on Earth's surface and I_{sp}

is the specific impulse. The same indirect optimization approach of the previous analysis is adopted for this problem. The Hamiltonian is the defined as

$$
\begin{aligned}
H = {} & \frac{2}{\pi}\frac{T}{m}\sqrt{\frac{a}{\mu}}\left(\pi\lambda_a a\cos\beta + \lambda_\imath\sin\beta\cos\vartheta_0 + \lambda_\Omega\sin\beta\frac{\sin\vartheta_0}{\sin\imath}\right) \\
& -\lambda_\Omega J_2\frac{3}{2}\left(\frac{r_E}{a}\right)^2\sqrt{\frac{\mu}{a^3}}\cos\imath - \lambda_m\frac{T}{c}
\end{aligned}
\tag{27}
$$

and the Euler-Lagrange equations are

$$
\begin{aligned}
\frac{\mathrm{d}\lambda_a}{\mathrm{d}t} = {} & -3\lambda_a a\frac{T}{m}\sqrt{\frac{1}{\mu a}}\cos\beta - \lambda_\imath\left[\frac{1}{\pi}\frac{T}{m}\sqrt{\frac{1}{\mu a}}\sin\beta\cos\vartheta_0\right] \\
& -\lambda_\Omega\left[\frac{1}{\pi}\frac{T}{m}\sqrt{\frac{1}{\mu a}}\sin\beta(\sin\vartheta_0/\sin\imath) + J_2\frac{21}{4}\left(\frac{r_E}{a}\right)^2\sqrt{\frac{\mu}{a^5}}\cos\imath\right]
\end{aligned}
\tag{28}
$$

$$
\frac{\mathrm{d}\lambda_\imath}{\mathrm{d}t} = \lambda_\Omega\left[\frac{2}{\pi}\frac{T}{m}\sqrt{\frac{a}{\mu}}\sin\beta\frac{\sin\vartheta_0}{\sin^2\imath}\cos\imath - J_2\frac{3}{2}\left(\frac{r_E}{a}\right)^2\sqrt{\frac{\mu}{a^3}}\sin\imath\right]
\tag{29}
$$

$$
\frac{\mathrm{d}\lambda_\Omega}{\mathrm{d}t} = 0
\tag{30}
$$

$$
\frac{\mathrm{d}\lambda_m}{\mathrm{d}t} = 2\frac{T}{m^2}\sqrt{\frac{a}{\mu}}\left[\lambda_a a\cos\beta + \lambda_\imath\frac{1}{\pi}\sin\beta\cos\vartheta_0 + \lambda_\Omega\frac{1}{\pi}\sin\beta\frac{\sin\vartheta_0}{\sin\imath}\right]
\tag{31}
$$

It is worth noting that a and $\imath$ can no more be treated as constant, as relevant changes characterize the multiple-revolution transfer.

The transfer control variables are β, ϑ_0 and the thrust magnitude T. First, the Hamiltonian derivative with respect to ϑ_0 is nullified to obtain

$$
\tan\vartheta_0 = \lambda_\Omega/(\lambda_\imath\sin\imath)
\tag{32}
$$

and then the same is done with respect to β to find

$$
\tan\beta = \frac{\lambda_i\cos\vartheta_0 + \lambda_\Omega\sin\vartheta_0/\sin\imath}{\pi a\lambda_a}
\tag{33}
$$

In this paper, a maximization problem is posed and either $-t_f$ (minimum time) or m_f (minimum propellant consumption) is maximized. The optimal controls must maximize the Hamiltonian in agreement with Pontryagin's Maximum Principle and the correct quadrants must be selected: $\cos\beta$ must have the same sign as λ_a and $\sin\beta$ as $\lambda_\imath\cos\vartheta_0 + \lambda_\Omega\sin\vartheta_0/\sin\imath$. One can arbitrarily select $\sin\beta > 0$ (i.e., β between 0 and 180 degrees) and correspondingly select the quadrant for ϑ_0 to finally obtain

$$
\begin{aligned}
\sin\beta &= \Lambda/\sqrt{\Lambda^2 + (\pi a\lambda_a)^2} \tag{34}\\
\cos\beta &= \pi a\lambda_a/\sqrt{\Lambda^2 + (\pi a\lambda_a)^2} \tag{35}\\
\sin\vartheta_0 &= \lambda_\Omega/(\Lambda\sin\imath) \tag{36}\\
\cos\vartheta_0 &= \lambda_\imath/\Lambda \tag{37}
\end{aligned}
$$

It is worth noting that the optimal controls vary continuously with time, in contrast to the one revolution transfer. However, since they are based on an approximation of the differential equations governing the dynamical system (in turn obtained with the sub-optimal constant-beta control law), the control history will not be the actual optimal control law. Indeed, the objective of this paper is to demonstrate that this building-block method can be adopted for the fast evaluation of large sets of transfers. A more precise (and computationally slower) calculation of the optimal control law is beyond the scope of this study.

The Hamiltonian is linear with respect to the thrust magnitude and can be rewritten as

$$H = TS_F - \lambda_\Omega J_2 \frac{3}{2} \left(\frac{r_E}{a}\right)^2 \sqrt{\frac{\mu}{a^3}} \cos \iota \tag{38}$$

where the switching function S_F has been introduced

$$S_F = \frac{2}{\pi} \frac{1}{m} \sqrt{\frac{a}{\mu}} \sqrt{(\pi a \lambda_a)^2 + \lambda_i^2 + \left(\frac{\lambda_\Omega}{\sin \iota}\right)^2} - \frac{\lambda_m}{c} = \frac{2}{\pi} \frac{1}{m} \Lambda' - \frac{\lambda_m}{c} \tag{39}$$

The thrust assumes its maximum value when $S_F > 0$, whereas the engine must be turned off when $S_F < 0$, in agreement with Pontryagin's Maximum Principle.

The adjoint variables can be interpreted as influence functions [21], in the sense that, at any point of the trajectory, they represent the derivative of the performance index with respect to a change of the corresponding variable. As a general trend, an adjoint variable has the same sign of the desired overall change of the corresponding variable, but, locally along the trajectory, it may also have the opposite sign. Large absolute values of an adjoint variable, signal the increased necessity/convenience of using thrust to change the corresponding state variable. Therefore, the relative ratio of λ_a and Λ determines the optimal split of the thrusting effort between in-plane and out-of-plane maneuvering, and ϑ_0 (related to the ratio between λ_i and λ_Ω) the preference between changing inclination or RAAN.

4. Optimization Problem

The actual control law depends on the boundary conditions that define the prescribed transfer and on the performance index. In this paper, the initial orbital elements a_0, ι_0, and Ω_0 are imposed; $\Omega_0 = 0$ is fixed by properly selecting the reference axis. The target orbit that must be reached at the end of the transfer is specified by its elements at the initial time $t_0 = 0$, that are a_T, ι_T, and Ω_{T0}. Target RAAN is perturbed by J2 with rate $(\dot{\Omega}_{J2})_T$ (function of a_T and ι_T only) and at the final time the following conditions must hold: $a_f = a_T$ (no drag acting on the target), $\iota_f = \iota_T$, and $\Omega_f = \Omega_{T0} + (\dot{\Omega}_{J2})_T t_f$.

The theory of optimal control also provides the boundary conditions for optimality [21, 22]. In the case of a minimum time trajectory with free final mass, the boundary conditions are $H_f - \lambda_\Omega (\dot{\Omega}_{J2})_T = 1$ and $\lambda_{mf} = 0$. In this case the switching function is always positive, and the engine is always on at

	Minimum final time	Maximum final mass
State equations	Eqs. 23, 24, 25, 26	
Euler-Lagrange equations	Eqs. 28, 29, 30, 31	
Boundary conditions	$a_f = a_T$	
	$i_f = i_T$	
	$\Omega_f = \Omega_{T0} + (\dot{\Omega}_{J2})_T t_f$	
	$\lambda_{mf} = 0$	$\lambda_{mf} = 1$
	$H_f - \lambda_\Omega(\dot{\Omega}_{J2})_T = 1$	$t_f = k$
Unknowns	$t_f, \lambda_{a0}, \lambda_{i0}, \lambda_{\Omega0}, \lambda_{m0}$	

Table 1: Optimization problem formulation

maximum thrust. The five boundary conditions at t_f determine the five problem unknowns, i.e., t_f and the initial values of the adjoint variables. The condition on the final value of the Hamiltonian is actually only a scaling condition, as the problem is homogeneous in the adjoint variables, and can be replaced by specifying one of the initial values, e.g., λ_Ω (which is constant). Note that the proper sign must be selected to avoid solutions with negative time-of-flight. As a rule of thumb, the sign of λ_Ω is the same as the difference between the perturbed RAAN values of the final and initial orbits, evaluated at the expected final time of Edelbaum's transfer (i.e., the transfer that neglects perturbations and RAAN) for the same changes of semimajor axis and inclination. In the case of maximum final mass, one has $\lambda_{mf} = 1$ (which becomes the scaling condition); the switching function can now become negative and the engine must be turned off when this condition occur. In addition, one has either $t_f = k$ for specified final time or $H_f - \lambda_\Omega(\dot{\Omega}_{J2})_T = 0$ for free final time. It is worth noting that this conditions is equivalent to $S_{Ff} = 0$, as the $J2$ perturbation on spacecraft and target is obviously the same at rendezvous.

The optimization problem formulation is summarized in Table 1, both for the minimum final time and maximum final mass problems.

In some cases, a decrease of the orbit altitude is required to increase the effect of J2 perturbation on the spacecraft, which may penetrate the atmosphere. A constrained optimization problem must be defined in this case, by fixing a minimum altitude constraint (e.g., $h_{lim} = 200$ km). When the constraint must be introduced, a three-arc structure becomes optimal. The spacecraft follows the optimal control law during the initial and final arcs, from t_0 to t_1 and from t_2 to t_f. It flies at constant altitude (i.e., with $\beta = 90$ deg) during the intermediate arc from t_1 to t_2. The height constraint is conveniently enforced at point 2, where the additional boundary condition $a_2 = r_E + h_{lim}$ is introduced. The boundary conditions for optimality state continuity for H and adjoint variables at both t_1 and t_2, except λ_{a2} which has a free discontinuity. From Hamiltonian continuity at t_1 one derives $\lambda_{a1-} = 0$ (subscripts - and + distinguish values just before and after the relevant point when a discontinuity occurs). In a similar way, At t_2 one has $\lambda_{a2+} = 0$. The three boundary conditions on a_2, λ_{a1-}, and λ_{a2+} determine the three additional unknowns t_1, t_2, and λ_{a2+}. It is worth

	Minimum final time	Maximum final mass
State equations	Eqs. 23, 24, 25, 26	
Euler-Lagrange equations	Eqs. 28, 29, 30, 31	
Boundary conditions	$a_f = a_T$	
	$i_f = i_T$	
	$\Omega_f = \Omega_{T0} + (\dot{\Omega}_{J2})_T t_f$	
	$a_2 = r_E + h_{lim}$	
	$\lambda_{a1-} = 0$	
	$\lambda_{a2+} = 0$	
	$\lambda_{mf} = 0$	$\lambda_{mf} = 1$
	$H_f - \lambda_\Omega(\dot{\Omega}_{J2})_T = 1$	$t_f = k$
Unknowns	$t_1, t_2, t_f, \lambda_{a0}, \lambda_{a2+}, \lambda_{i0}, \lambda_{\Omega0}, \lambda_{m0}$	

Table 2: Optimization problem formulation with altitude constraint

noting that λ_a does not influence the equations and control laws during the constrained arc ($\cos\beta = 0$); the integration of the corresponding differential equation can be omitted during this arc. The resulting optimization problem formulation is summarized in Table 2.

The physical meaning of the adjoint variables allows for interesting observations. In Edelbaum's problem (no perturbations and no constraint on Ω), λ_Ω is zero and λ_i is constant. When the spacecraft is moving outward (positive λ_a and $\cos\beta$) λ_a has a negative derivative and β grows, as the plane change is less expensive far from the Earth. The well-known relation $\sin\beta \propto 1/V$, which characterizes Edelbaum's problem, can be easily demonstrated by reformulating the problem with a or V as the independent variable [11]. Note that a non-monotonic change of a may be required, depending on the prescribed transfer, and therefore the formulation with time as the independent variable is preferred here to maintain a general solution. It should also be noted that, when $\lambda_\Omega = 0$, the switching function results to be constant. The minimum-propellant problem has therefore the switching function constantly null (singular arc) and the transfer cost does not depend on the thrust magnitude, as any value (even variable during the maneuver) leads to the same consumption (but different time of flight).

The Euler-Lagrange equations also reflect that a pure change change in Ω, with same initial and final inclination, is not performed at constant $\imath$. For direct orbits ($\cos\imath > 0$), the derivative of $\lambda_\imath$ is positive, meaning that the inclination adjoint variable must initially be negative ($\imath$ is reduced) and then turns positive ($\imath$ is increased and returned to the initial value). This strategy reflects the fact that the cost of RAAN change is smaller for an orbit plane close to the equator. As a matter of fact, the optimal maneuver minimizes the rotation of angular momentum, and does not follow a constant-$\imath$ path. Similar observations pertain to retrograde orbits.

The effect of J2 appears when a constraint on the final RAAN value is imposed and λ_Ω is not equal to zero. The case of a direct orbit and a RAAN

increase ($\lambda_\Omega > 0$) is used as an example. The derivative of both λ_a and $\lambda_\imath$ have an additional negative contribution, compared to the non-perturbed case. In the case of no overall changes of both semimajor axis and inclination, λ_a and $\lambda_\imath$ are therefore initially positive and then become negative: a and $\imath$ are initially increased to reduce the negative Ω drift caused by J2, which obviously contrasts the required RAAN change. Similar observations can be made in the other cases.

5. Aerodynamic Drag and Drag Sail

The presence of aerodynamic forces is treated with the same approach used for the zero-drag transfer. Lift is usually negligible and only the effects of drag will be analyzed in this work. The perturbing acceleration due to drag $\boldsymbol{D}$ is given by

$$\frac{\mathrm{d}\boldsymbol{v}}{\mathrm{d}t} = \frac{\boldsymbol{D}}{m} = \frac{1}{2}\frac{\rho C_D S}{m} v_{rel}^2 \frac{\boldsymbol{v}_{rel}}{v_{rel}} \tag{40}$$

where C_D (typically close to 2.2) is the drag coefficient associated with the surface S, ρ is the atmospheric density. The velocity relative to atmosphere $\boldsymbol{v}_{rel}$ differs from the inertial velocity $\boldsymbol{v}$ as because of Earth rotation ω_E and

$$\boldsymbol{v}_{rel} = \boldsymbol{v} - \boldsymbol{\omega}_E \times \boldsymbol{r} \tag{41}$$

with magnitude

$$v_{rel} = \sqrt{\left(\sqrt{\frac{\mu}{a}} - \omega_E a \cos\imath\right)^2 + (\omega_E a \sin\imath\cos\vartheta)^2} \tag{42}$$

The effect of drag can solely be roughly estimated as the atmospheric density has a large variability. The 1976 U.S. Standard Atmosphere is adopted here. The optimization method is however independent of the atmospheric model, and can be readily adapted to different models. The full details on how the model is built are in [23]. Using the tabulated data, the density profile $\rho(z)$ between altitudes from $z = 86$km and $z = 1000$km can be calculated with the basic equation form

$$\rho(z) = \exp(Az^4 + Bz^3 + Cz^2 + Dz + E) \tag{43}$$

where the value of the coefficients are listed in table 3.

Gauss' planetary equations under the sole influence of aerodynamic drag $\boldsymbol{D}$ are

$$\frac{\mathrm{d}a}{\mathrm{d}t} = 2\frac{a}{V}\frac{D_V}{m} \tag{44}$$

$$\frac{\mathrm{d}\imath}{\mathrm{d}t} = \frac{1}{V}\frac{D_W}{m}\cos\vartheta \tag{45}$$

$$\sin\imath\frac{\mathrm{d}\Omega}{\mathrm{d}t} = \frac{1}{V}\frac{D_W}{m}\sin\vartheta \tag{46}$$

where drag components along the velocity vector D_V and perpendicular to the orbit plane D_W are introduced. The out-of-plane component is related to the Earth and atmosphere rotation by Eq. (41) and, after algebraic manipulation, the drag components are written as

$$D_V = -\frac{\rho S C_D}{2}\left(\sqrt{\frac{\mu}{a}} - \omega_E a\cos\imath\right)\sqrt{\left(\sqrt{\frac{\mu}{a}} - \omega_E a\cos\imath\right)^2 + (\omega_E a\sin\imath\cos\vartheta)^2}$$
(47)

$$D_W = -\frac{\rho S C_D}{2}\left(\omega_E a\sin\imath\cos\vartheta\right)\sqrt{\left(\sqrt{\frac{\mu}{a}} - \omega_E a\cos\imath\right)^2 + (\omega_E a\sin\imath\cos\vartheta)^2}$$
(48)

The differential equations with drag effect are averaged over one revolution using the average between minimum and maximum values reached during one revolution for v_{rel}

$$v_{rel} = 0.5\left(\sqrt{\frac{\mu}{a}} - \omega_E a\cos\imath\right) + 0.5\sqrt{\left(\sqrt{\frac{\mu}{a}} - \omega_E a\cos\imath\right)^2 + (\omega_E a\sin\imath)^2} \quad (49)$$

One should note that D_W is an even function and its effect on Ω vanishes over one revolution, as the right-hand side of Eq. (48) results to be odd.

The averaged contributions of drag are added to thrust and J2 contributions to obtain the differential system

$$\frac{\mathrm{d}a}{\mathrm{d}t} = 2\frac{T}{m}\sqrt{\frac{a^3}{\mu}}\cos\beta + \rho\frac{SC_D}{m}v_{rel}a\left(\sqrt{\frac{a^3}{\mu}}\omega_E\cos\imath - 1\right) \qquad (50)$$

$$\frac{\mathrm{d}\imath}{\mathrm{d}t} = \frac{2}{\pi}\frac{T}{m}\sqrt{\frac{a}{\mu}}\sin\beta\cos\vartheta_0 - \frac{1}{4}\sqrt{\frac{a^3}{\mu}}\rho\frac{SC_D}{m}v_{rel}\omega_E\sin\imath \qquad (51)$$

$$\frac{\mathrm{d}\Omega}{\mathrm{d}t} = \frac{2}{\pi}\frac{T}{m}\sqrt{\frac{a}{\mu}}\frac{\sin\beta}{\sin\imath}\sin\vartheta_0 - \frac{3}{2}J_2\left(\frac{r_E}{a}\right)^2\sqrt{\frac{\mu}{a^3}}\cos\imath \qquad (52)$$

$$\frac{\mathrm{d}m}{\mathrm{d}t} = -\frac{T}{c} \qquad (53)$$

Table 3: Density formula coefficients

Altitude, km	A	B	C	D	E
86-91	0.000000	-3.322622×10^{-6}	9.111460×10^{-4}	-0.2609971	5.944694
91-100	0.000000	2.873405×10^{-5}	-0.008492037	0.6541179	-23.62010
100-110	-1.240774×10^{-5}	0.005162063	-0.8048342	55.55996	-1443.338
110-120	0.000000	-8.854164×10^{-5}	0.03373254	-4.390837	176.5294
120-150	3.661771×10^{-7}	-2.154344×10^{-4}	0.04809214	-4.884744	172.3597
150-200	1.906032×10^{-8}	-1.527799×10^{-5}	0.004724294	-0.6992340	20.50921
200-300	1.199282×10^{-9}	-1.451051×10^{-6}	6.910474×10^{-4}	-0.1736220	-5.321644
500-750	8.105631×10^{-12}	-2.358417×10^{-9}	-2.635110×10^{-6}	-0.01562608	-20.02246
750-1000	$-3.701195 \times 10^{-12}$	-8.608611×10^{-9}	5.118829×10^{-5}	-0.06600998	-6.137674

The Hamiltonian becomes

$$
\begin{aligned}
H \;=\;& \lambda_a \left[2\frac{T}{m}\sqrt{\frac{a^3}{\mu}}\cos\beta + \rho\frac{SC_D}{m}v_{rel}\,a\left(\sqrt{\frac{a^3}{\mu}}\,\omega_E\cos\imath - 1\right)\right] + \\
&+\lambda_\imath \left[\frac{2}{\pi}\frac{T}{m}\sqrt{\frac{a}{\mu}}\sin\beta\cos\vartheta_0 - \frac{1}{4}\sqrt{\frac{a^3}{\mu}}\rho\frac{SC_D}{m}v_{rel}\omega_E\sin\imath\right] + \\
&+\lambda_\Omega \left[\frac{2}{\pi}\frac{T}{m}\sqrt{\frac{a}{\mu}}\frac{\sin\beta}{\sin\imath}\sin\vartheta_0 - \frac{3}{2}J_2\left(\frac{r_E}{a}\right)^2\sqrt{\frac{\mu}{a^3}}\cos\imath\right] + \\
&-\lambda_m\frac{T}{c}
\end{aligned}
\tag{54}
$$

and the Euler-Lagrange equations, with v_{rel} averaged over one revolution, are

$$
\begin{aligned}
\frac{\mathrm{d}\lambda_a}{\mathrm{d}t} \;=\;& -\lambda_a 3\frac{T}{m}\sqrt{\frac{a}{\mu}}\cos\beta \\
&+\lambda_a\frac{SC_D}{m}\left(\rho v_{rel} + a\frac{\partial\rho}{\partial a}v_{rel} + a\rho\frac{\partial v_{rel}}{\partial a}\right) \\
&-\lambda_a\frac{SC_D}{m}\frac{\omega_E}{n_{S/C}}\cos\imath\left(\frac{5}{2}\rho v_{rel} + a\frac{\partial\rho}{\partial a}v_{rel} + a\rho\frac{\partial v_{rel}}{\partial a}\right) \\
&-\lambda_\imath\frac{1}{\pi}\frac{T}{m}\frac{1}{\sqrt{a\mu}}\sin\beta\cos\vartheta_0 \\
&+\frac{\lambda_\imath}{4}\frac{SC_D}{m}\frac{\omega_E}{n_{S/C}}\sin\imath\left(\frac{3}{2}\frac{\rho}{a}v_{rel} + \frac{\partial\rho}{\partial a}v_{rel} + \rho\frac{\partial v_{rel}}{\partial a}\right) \\
&-\lambda_\Omega\left[\frac{1}{\pi}\frac{T}{m}\frac{1}{\sqrt{a\mu}}\frac{\sin\beta}{\sin\imath}\sin\vartheta_0 + \frac{21}{4}J_2\left(\frac{r_E}{a}\right)^2\frac{n_{S/C}}{a}\cos\imath\right]
\end{aligned}
\tag{55}
$$

$$
\begin{aligned}
\frac{\mathrm{d}\lambda_\imath}{\mathrm{d}t} \;=\;& \lambda_a a\left[\rho\frac{SC_D}{m}\frac{\partial v_{rel}}{\partial\imath} - \rho\frac{SC_D}{m}\frac{\omega_E}{n_{S/C}}\left(\frac{\partial v_{rel}}{\partial\imath}\cos\imath - v_{rel}\sin\imath\right)\right] \\
&+\frac{\lambda_\imath}{4}\rho\frac{SC_D}{m}\frac{\omega_E}{n_{S/C}}\left(v_{rel}\cos\imath + \frac{\partial v_{rel}}{\partial\imath}\sin\imath\right) \\
&+\lambda_\Omega\left[\frac{2}{\pi}\frac{T}{m}\sqrt{\frac{a}{\mu}}\sin\beta\frac{\sin\vartheta_0}{\sin^2\imath}\cos\imath - \frac{3}{2}J_2\left(\frac{r_E}{a}\right)^2 n_{S/C}\sin\imath\right]
\end{aligned}
\tag{56}
$$

$$
\frac{\mathrm{d}\lambda_\Omega}{\mathrm{d}t} \;=\; 0
\tag{57}
$$

$$
\begin{aligned}
\frac{\mathrm{d}\lambda_m}{\mathrm{d}t} \;=\;& \lambda_a a\left[2\frac{T}{m^2}\sqrt{\frac{a}{\mu}}\cos\beta + \rho\frac{SC_D}{m^2}v_{rel}\left(\frac{\omega_E}{n_{S/C}}\cos\imath - 1\right)\right] \\
&+\lambda_\imath\left[\frac{2}{\pi}\frac{T}{m^2}\sqrt{\frac{a}{\mu}}\sin\beta\cos\vartheta_0 - \frac{1}{4}\rho\frac{SC_D}{m^2}v_{rel}\frac{\omega_E}{n_{S/C}}\sin\imath\right] \\
&+\lambda_\Omega\frac{2}{\pi}\frac{T}{m^2}\sqrt{\frac{a}{\mu}}\frac{\sin\beta}{\sin\imath}\sin\vartheta_0
\end{aligned}
\tag{58}
$$

The expressions for $\partial v_{rel}/\partial a$, $\partial v_{rel}/\partial \imath$ and $\partial \rho/\partial a$ are given by:

$$\frac{\partial v_{rel}}{\partial a} = -\frac{1}{4}n_{S/C} - \frac{\omega_E}{2}\cos\imath +$$
$$- \frac{\left(n_{S/C} - \omega_E\cos\imath\right)\left(\frac{1}{2}n_{S/C} + \omega_E\cos\imath\right) - \left(\omega_E\sin\imath\right)^2}{2\sqrt{\left(n_{S/C} - \omega_E\cos\imath\right)^2 + \left(\omega_E\sin\imath\right)^2}} \tag{59}$$

$$\frac{\partial v_{rel}}{\partial \imath} = \frac{\omega_E a\sin\imath}{2}\left[1 + \frac{n_{S/C}}{\sqrt{\left(n_{S/C} - \omega_E\cos\imath\right)^2 + \left(\omega_E\sin\imath\right)^2}}\right] \tag{60}$$

$$\frac{\partial \rho}{\partial a} = \rho\left[4A\left(a - r_E\right)^3 + 3B\left(a - r_E\right)^2 + 2C\left(a - r_E\right) + D\right] \tag{61}$$

where r_E is the radius of the Earth and the coefficients A, B, C and D depend on the altitude as described in Table 5.

The formal expressions for the optimal controls do not change for thrust magnitude and angles; β, ϑ_0, and the switching function are again given by Eqs. (34)-(37), and Eq. (39). The Hamiltonian is linear with respect to the thrust magnitude and also to the sail area, which can be considered an additional control variable for a deployable/retractable sail. By introducing the spacecraft mean motion $n_{S/C} = \sqrt{\mu/a^3}$, H is rewritten as

$$H = S_F T + S_S S - \lambda_\Omega\frac{3}{2}J_2\left(\frac{r_E}{a}\right)^2 n_{S/C}\cos\imath \tag{62}$$

where S_S is introduced to denote the sail switching function:

$$S_S = \rho\frac{C_D}{m}v_{rel}\left[\lambda_a a\left(\frac{\omega_E}{n_{S/C}}\cos\imath - 1\right) - \lambda_\imath\frac{1}{4}\frac{\omega_E}{n_{S/C}}\sin\imath\right] \tag{63}$$

The frontal area must assume its maximum value, that is the drag sail is fully deployed, when $S_S > 0$. On the other hand, the frontal area must assume its minimum value, that is the drag sail is retracted, when $S_S < 0$. One should note that $\omega_E/n_{S/C} << 1$, and S_S is approximately proportional to $-\lambda_a$.

The enforcement of the altitude constraint is more complex when drag is considered, as the simple condition $\cos\beta = 0$ during flight at constant altitude is now replaced by

$$\cos\beta = \sqrt{\frac{\mu}{a}}\frac{\rho S C_D}{2T}v_{rel}\left(1 - \frac{\omega_E}{n_{S/C}}\cos\imath\right) = D_a/T \tag{64}$$

which states that thrust along the inertial velocity must equate the average drag in this direction: $T\cos\beta = D_a$. The thruster must be on and $\cos\beta > 0$ is required to contrast drag. During the constrained arc the Hamiltonian must be redefined to take the constraint into account

$$H = S_F T + S_S S - \lambda_\Omega\frac{3}{2}J_2\left(\frac{r_E}{a}\right)^2 n_{S/C}\cos\imath$$
$$+ \nu\left[2\frac{T}{m}\sqrt{\frac{a^3}{\mu}}\cos\beta + \rho\frac{S C_D}{m}v_{rel}a\left(\sqrt{\frac{a^3}{\mu}}\omega_E\cos\imath - 1\right)\right] \tag{65}$$

14

with ν an arbitrary constant, as it is multiplied by an identically zero term. Note that H coincide with Eq. (54), but $\lambda_a + \nu$ must replace λ_a. The combination of ν, T, β, ϑ_0, and S that maximizes H while satisfying the constraint must be selected. The optimality conditions for β and ϑ_0 do not change but $\lambda_a + \nu$ replaces λ_a in Eqs. (34) and (35), and, in a similar way, $\lambda_a + \nu$ appears in S_F and S_S. The term $\lambda_a + \nu$ must be positive to ensure the correct thrust direction; for this reason, S_S is always negative ($\omega_E << n_{S/C}$ and only large negative λ_i values, never encountered in the problems treated in this article, could make S_S positive). The sail is therefore always retracted during flight at constant altitude.

By expressing $\cos\beta = \pi a(\lambda_a + \nu)/\Lambda'$ and $\sin\beta = \Lambda/\Lambda'$ one can easily rewrite the switching function

$$S_F = \frac{1}{\sin\beta}\frac{2}{\pi}\frac{1}{m}\sqrt{\frac{a}{\mu}}\sqrt{\lambda_i^2 + \left(\frac{\lambda_\Omega}{\sin\imath}\right)^2} - \frac{\lambda_m}{c} \tag{66}$$

which now implicitly depends on thrust and sail drag, since the relation $\sin\beta = \sqrt{1 - (D_a/T)^2}$ must hold. Two cases are possible to maximize H. Either $T = T_{max}$ and the thrust angle is obtained from $\sin\beta = \sqrt{1 - (D_a/T_{max})^2}$ when the corresponding $S_F > 0$, or

$$\sin\beta = \frac{2}{\pi}\frac{c}{m\lambda_m}\sqrt{\frac{a}{\mu}}\sqrt{\lambda_i^2 + \left(\frac{\lambda_\Omega}{\sin\imath}\right)^2} \tag{67}$$

and the thrust magnitude is given by $T = D_a/\cos\beta$ when S_F evauated at T_{max} is negative. For minimum-time problems maximum thrust must be used as S_F is always positive.

As far as the boundary conditions are concerned, Hamiltonian continuity requires $\cos\beta$ to be continuous, that, is,

$$\sqrt{\frac{\mu}{a_1}}\frac{\rho SC_D}{2T}v_{rel1}\left(1 - \frac{\omega_E}{n_{S/C1}}\cos\imath_1\right) = \frac{\pi a_1\lambda_{a1}}{\sqrt{\Lambda_1^2 + (\pi a_1\lambda_{a1})^2}} \tag{68}$$

$$\sqrt{\frac{\mu}{a_2}}\frac{\rho SC_D}{2T}v_{rel2}\left(1 - \frac{\omega_E}{n_{S/C2}}\cos\imath_2\right) = \frac{\pi a_2\lambda_{a2+}}{\sqrt{\Lambda_2^2 + (\pi a_2\lambda_{a2+})^2}} \tag{69}$$

These optimality conditions and the altitude limit implicitly determine the three additional unknowns t_1, t_2 and λ_{a2+}, as summarized in table 4. Note that λ_a must be actually integrated during the constrained arc, as it appears in the other differential equations.

6. Boundary value problem solution

The boundary value problem is here solved with an iterative procedure which uses Newton's method to bring the errors to zero. First of all, tentative values

	Minimum final time	Maximum final mass
State equations	Eqs. 50, 51, 52, 53	
Euler-Lagrange equations	Eqs. 55, 56, 57, 58	
Boundary conditions	$a_f = a_T$ $i_f = i_T$ $\Omega_f = \Omega_{T0} + (\dot{\Omega}_{J2})_T t_f$ $a_2 = r_E + h_{lim}$ Eqs. 68, 69	
	$\lambda_{mf} = 0$	$\lambda_{mf} = 1$
	$H_f - \lambda_\Omega(\dot{\Omega}_{J2})_T = 1$	$t_f = k$
Unknowns	$t_1, t_2, t_f, \lambda_{a0}, \lambda_{a2+}, \lambda_{i0}, \lambda_{\Omega 0}, \lambda_{m0}$	

Table 4: Optimization problem formulation with altitude constraint (drag)

are assumed for the unknowns. They are collected in vector $\mathbf{p}$. Then, the differential equations are integrated. The authors here used the Adams-Moulton variable-step and variable-order integration scheme, as it is more suitable to deal with thrust discontinuities than a fixed-step scheme. After the integration, the errors $\boldsymbol{\Psi}$ on the boundary conditions are found. Under linear approximation, the correction of the tentative values must be

$$\Delta \mathbf{p} = -K_1 \left[\frac{\partial \boldsymbol{\Psi}}{\partial \mathbf{p}} \right]^{-1} \boldsymbol{\Psi} \tag{70}$$

The matrix in (70) is numerically evaluated. The variation of the boundary conditions $\Delta \Psi$ is computed by varying each unknown by a small amount Δp ($10^{-6} \div 10^{-7}$) while keeping the others fixed and by integrating the equations. The i-th row of the matrix can be approximated by $\Delta \Psi^T / \Delta p$. The relaxation factor K_1(between 0 and 1) avoids moving away from the solution when large theoretical corrections are computed.

Indirect methods may suffer from poor convergence. It is therefore of the utmost importance that the initial guess is sufficiently close to the optimal solution in order for the method to converge. A continuation scheme was here adopted to solve this issue. Given the parameters of initial and final orbit, the minimum time solution is first achieved, and the maximum final mass solutions are then evaluated by gradually increasing the transfer time. The initial values of the current converged solution are taken as initial guess for the next transfer. This ensures that the tentative values are heuristically close enough to the optimal ones. User's experience helps to find the initial tentative values of the minimum time solutions, which have a simpler convergence as no engine switch is present. Edelbaum's solution, neglecting RAAN change, can be used to estimate the arrival time, at which the RAAN difference between chaser and target is evaluated. This value, in turn, suggests which changes of semimajor axis and inclination help reducing the difference and therefore the sign of the initial values of the corresponding adjoint variables. Arbitrary magnitudes (e.g., equal to unity) can be assigned to them; different magnitude combinations can

be tried if convergence is not obtained.

7. Results

Drag is initially neglected and minimum-time solutions are presented first; selected minimum-propellant trajectories are then discussed. Minimum-time and minimum-propellant solutions with drag with be finally presented. The initial orbit altitude is fixed at 400 km with initial inclination of 51.6 degrees (ISS). A small 15-kg spacecraft is considered; available thrust is 10 mN with a specific impulse of 2500 s.

7.1. Minimum-Time Solutions

Better insight can be obtained with a simpler problem, and trajectories with constant acceleration are initially considered. In this case, the solutions result to be perfectly symmetric when altitude and inclination change are 0; the adjoint variables reach 0 and change sign at the mid-point, and the thrust angles during the second half are specular with respect to the first half. The constant-acceleration case (i.e., $c = \infty$) is initially adopted to obtain minimum-time solutions. For constant mass and acceleration, the equations for m and λ_m can be neglected.

The transfer is characterized by the values of a_0, a_f, $\imath_0$ and $\imath_f$, and by the relative RAAN angle $\Delta\Omega_0 = \Omega_{T0} - \Omega_0$ at t_0. For each combination of a_0, a_f, $\imath_0$ and $\imath_f$, there is an optimal value of initial phase angle $\Delta\Omega^*$ that corresponds to a global minimum of flight time (and propellant consumption). The global minimum is found by letting Ω_{T0} free, leading to boundary condition for optimality $\lambda_\Omega = 0$. In this case, thrust is only used to attain the prescribed final values of a and $\imath$, while Ω reaches Ω_T thanks to the effect of $J2$ only.

The trip time grows if the initial phase angle $\Delta\Omega_0$ is different from $\Delta\Omega^*$; part of the thrusting effort must now be used also to change Ω, both directly and with a different strategy that modifies a and $\imath$ histories in order to exploit $J2$. The results for transfers with an altitude change of -200 km and different values of inclination changes are shown in Figure 1. The value of Ω_{T0} for the globally optimal solution is close to 1 degree in the three cases, even though slightly different values pertain to each curve. At the selected altitude and inclination, J2 perturbation is modified more effectively by changing a rather than $\imath$, and the optimal strategies follows this guideline to attain the required RAAN. Figure 2 presents semimajor axis and inclination histories for $\Omega_{T0} = \pm 10$ degrees: when $\Delta\Omega_0 > \Delta\Omega^*$ (by a sufficiently large margin), a is initially increased to reduce the effect of $J2$ on the chaser spacecraft, thus bringing the orbit nodes closer. A reduction of $\imath$ is also beneficial because it reduces the cost of changing Ω; therefore the trip time is lower when $\Delta\imath$ is negative, whereas an imposed increase in $\imath$ acts unfavorably. On the other hand, when $\Delta\Omega_0 < \Delta\Omega^*$ the spacecraft semimajor axis should be reduced below the target value, but this is not allowed by the presence of the atmosphere. The RAAN change must now be obtained mainly by the direct use of thrust, which is more effective if
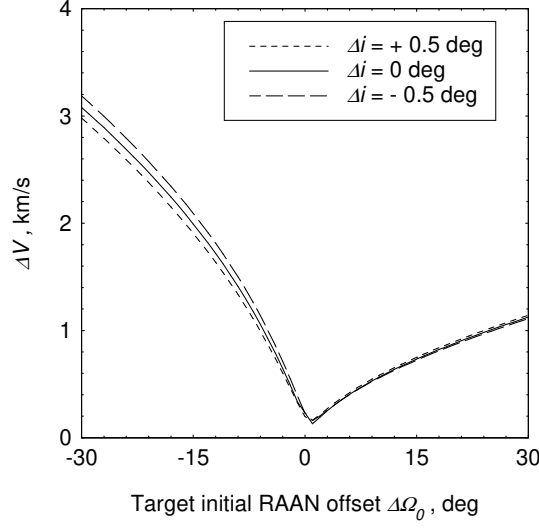
Figure 1: Minimum trip time as a function of the target initial RAAN offset.
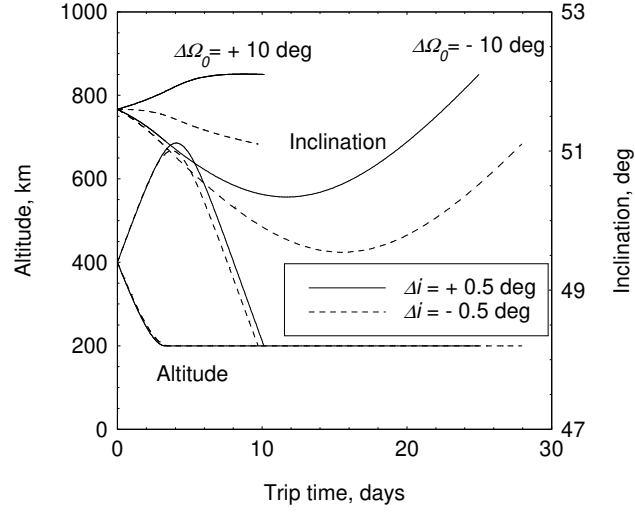

Figure 2: Minimum-time trajectories for $\Delta a = -200$ km and $\Delta \Omega_0 = 10$ degrees.

the inclination is reduced. However, the increased $J2$ effect on the chaser at lower inclination is in contrast to the required RAAN change, and the maneuver with $i_T < i_0$ results to be less efficient and longer. Minimum-time missions with variable mass exhibit similar behavior; the symmetry of the solutions is however lost, due to the changing acceleration.
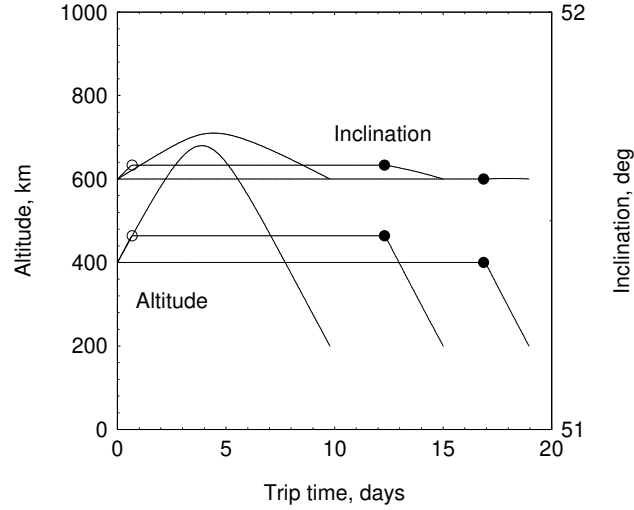
Figure 3: Minimum-propellant trajectories for $\Delta a = -200$ km and $\Delta\Omega_0 = +10$ degrees (full circle = thruster on, empty circle = thruster off).

7.2. Minimum-Propellant Solutions - No Drag

The thruster is always on in minimum-time solutions, but the introduction of coasting arcs may be beneficial in terms of propellant consumption. As a matter of fact, if sufficient time is available, the chaser can wait for the angle between the orbit planes to become $\Delta\Omega^*$ and then perform the globally optimal transfer defined in the previous subsection. For shorter available times, minimum-propellant solutions become of interest.

Two different structures for the optimal solution are found, depending on the orbit characteristics, or, more precisely, on whether $\Delta\Omega$ is changing towards of moving away from $\Delta\Omega^*$. The first possibility arises when the chaser and target orbit planes are moved closer by the effect of J2: the case of a -200 km change of semimajor axis, constant inclination, and $\Omega_{T0} = 10$ degrees, is used as an example. Solutions for different time of flight are compared in Fig. 3. The minimum-time solution sets a lower bound on the time of flight. If the available time is increased from this value (which is about 10 days for this case), a coast arc appears to separate two burns. The required increase of semimajor axis is reduced compared to the minimum-time solution, as time can now be spent on a suitable orbit where the spacecraft waits for J2 to make the orbital planes closer (e.g., 15-day solution in Fig. 3). For time of flight close to 19 days, the initial burn vanishes and the global-optimum solution can be flown after waiting on the initial orbit for about 17 days. The propellant consumptions are compared in Table 5.

An opposite situation occurs when the angle between the orbit planes is increased by J2 effect, as when the required change of semimajor axis is positive. As an example, the case of a +200 km change of semimajor axis, again with
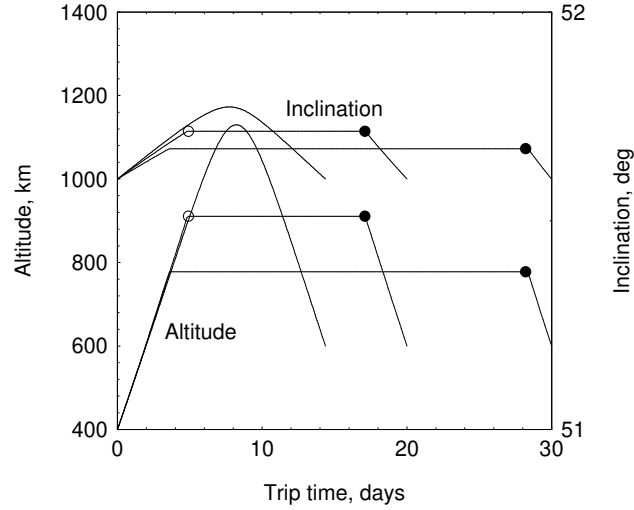
Figure 4: Minimum-propellant trajectories for $\Delta a = +200$ km, $\Delta\Omega_0 = 10$ degrees and $\Delta\Omega_f = 0$ (full circle = thruster on, empty circle = thruster off).

constant inclination and $\Omega_{T0} = 10$ degrees, is presented. The strategy of waiting on the initial orbit is not suitable (unless a complete revolution is performed in the node relative motion). Solutions for different time of flight are shown in Fig. 4. The minimum-time solution (about 14.5 days) requires an increase of semimajor axis beyond the target value to change the sign of the nodes relative motion. If the time of flight is increased, a coast arc is again introduced at a suitable height to wait for J2 to make the orbit plane closer. The 20-day and 30-day solutions are shown in Fig 4.

The trajectory structure is symmetrical to the case with a semimajor axis reduction. However, these solutions cannot reach the global optimum unless time grows to infinity, with a slowly decreasing propellant consumption as time is increased. As a matter of fact, if sufficient time is allowed, a different strategy becomes available; instead of contrasting the relative node motion of the initial orbit with respect to the target, one can favor it, that is, instead of reducing $\Delta\Omega$ to 0, it is increased to 2π. Example solutions are shown in Fig. 5.

For relatively short times of flight (e.g., 200 days), this strategy initially reduces the semimajor axis to the minimum altitude; the constant-altitude flight shows a coasting arc that separates two burns that actively correct Ω (and $\imath$); the mission cost is quite large (1.8 kg). For longer times of flight (e.g., 300 days) thrust is not used on the constant-altitude flight, where instead the spacecraft waits for J2 to perform the plane change. For even longer times (400 days), the minimum altitude is not reached and the waiting orbit is between the minimum and the initial orbit. The propellant consumption has decreased to 0.168 kg for this solution. Finally, the waiting orbit becomes the initial orbit and the global optimum is reached; in this case, however, almost two years (725 days)
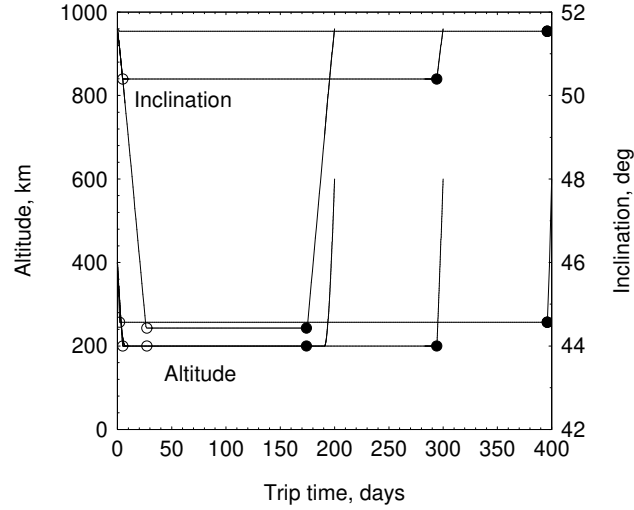
Figure 5: Minimum-propellant trajectories for $\Delta a = +200$ km, $\Delta \Omega_0 = 10$ degrees and $\Delta \Omega_f = 2\pi$ (full circle = thruster on, empty circle = thruster off).

are required to attain this optimal solution. The trip time at which this strategy bests the solution that takes $\Delta \Omega$ to 0 instead of 2π obviously depends on the initial $\Delta \Omega$; in this case, with $\Delta \Omega_0$ only at 10 degrees, about 700 days are required. It is interesting to note how the altitude change limitations due to the atmosphere force the search for large inclinations changes to achieve the required J2 effect on the orbit.

Table 5: Propellant consumption for $\Delta a = \pm 200$ km, $\Delta i = 0$ and $\Delta \Omega_0 = 10$.

	Trip time, days	Propellant consumption, kg
	10 (minimum)	0.345
$\Delta a = -200$ km	15	0.117
	19 (global optimum)	0.071
	Trip time, days	Propellant consumption, kg
	14.5 (minimum)	0.507
$\Delta a = +200$ km	20	0.272
	30	0.170
	725 (global optimum)	0.068

7.3. Transfers with Drag Sail

Drag can profitably be exploited to reduce the altitude when required. Drag adds to thrust during braking phases in minimum-time solutions, reducing trans-
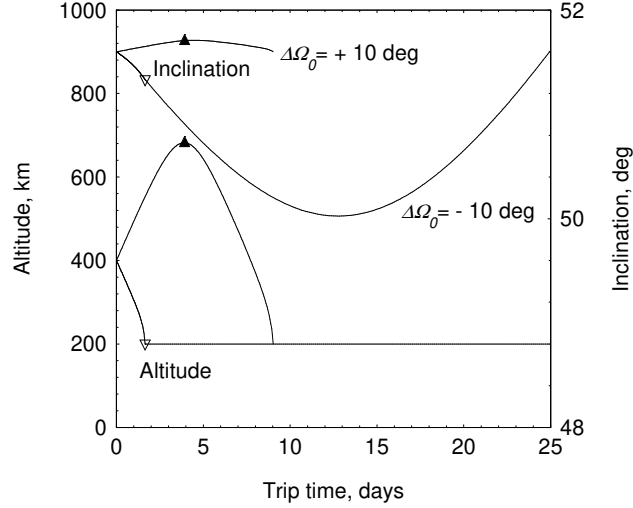
21

Figure 6: Minimum-time trajectories with dragsail for $\Delta a = -200$ km (full triangle = sail is opened).

fer time and saving propellant. If sufficient time is available, in minimum-propellant solutions drag is used instead of thrust during the braking phases, further reducing the propellant consumption. Numerical results consider a spacecraft frontal area (sail retracted) equal to 0.04m^2 and an open sail area of 4m^2. $C_D = 2.2$ in both cases.

Figure 6 compares minimum time trajectories for $\Delta a = -200$ km, $\Delta i = 0$ km, and $\Delta\Omega_0 = \pm 10$ degrees. Node regression is larger for the target (lower altitude) and the orbit planes are moving closer for $\Delta\Omega_0 = +10$ degrees. The optimal maneuver uses thrust to increase altitude and enhance the regression rate difference, and then both thrust and drag to attain the lower target orbit. An opposite strategy is used for $\Delta\Omega_0 = -10$ degrees, but the transfer time is larger as initial and target orbit planes are moving apart. In addition, the altitude constraint limits the regression rate difference that can be achieved, and thrust must be exploited to actively rotate the orbit plane. Inclination is reduced (again, using thrust) to keep the rotation cost lower. It is worth noting that the sail is always closed at an altitude slightly higher than the limiting value. The same characteristics can be found in Figure 7, where trajectories for $\Delta a = +200$ km are presented.

Figures 8 shows minimum-propellant trajectories for $\Delta a = -200$ km, $\Delta i = 0$, and $\Delta\Omega_0 = +10$ degrees (orbits moving closer). The optimal strategy uses a short initial thrusting arc to increase altitude and regression rate difference for transfer times above the minimum value (e.g. 14 days). The thruster is then turned off and the chaser waits for J2 to act, first with the sail closed and then with an open sail. Due to the large altitude, drag has a minimal effect, and the thruster must then be turned on again to attain the target orbit in
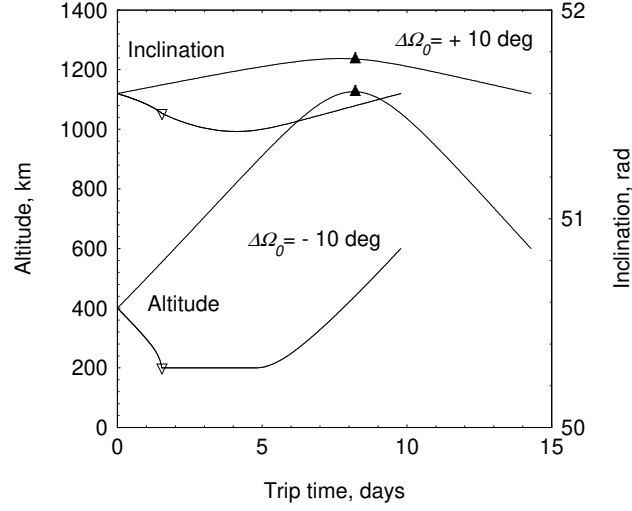
Figure 7: Minimum-time trajectories with dragsail for $\Delta a = +200$ (full triangle = sail is opened).

the prescribed time; only when altitude becomes sufficiently small, the thruster can be turned off again and the final descent is accomplished with drag only. The global optimum is attained at about 18 days. The propellant consumption would be zero if drag had no effect on inclination: the chaser could wait on the initial orbit for the proper orbit alignment and then use the sail alone to reduce the altitude to the target value. However, the small drag influence on inclination requires a very short initial thrusting arc to compensate for this effect; on the other hand, descent to the final altitude only requires an open sail and no thrusting is needed after this short initial arc.

For $\Delta a = +200$ km, $\Delta i = 0$, and $\Delta\Omega_0 = -10$ (again, orbits moving closer) and time of flight slightly above the minimum, the constant-altitude phase is flown at full thrust only in the initial part; at a given time, which depends on the available time of flight, the optimal control switches from $T = T_{max}$, $\cos\beta = D_a/T_{max}$ and $\sin\beta = \sqrt{1 - (D_a/T_{max})^2}$, to $\sin\beta$ given by Eq. (67). Thrust then returns at the maximum value at the end of the constant-altitude phase to start the ascent to the final orbit. When the available time of flight reaches about 11 days, the engine is turned off during the descent, and the remaining altitude reduction is obtained by the sail only. The engine is then turned on during the constant-altitude flight, again with reduced thrust. Thrust evolution for duration of 10, 10.5, 11 and 12 days are compared in figure 9. The sail is closed (triangles) shortly before the start of the constrained flight for trip time up to 11 days, but there is a long and slow descent phase with closed sail for a 12-day duration. In this case, the spacecraft still exploits a relatively large regression rate difference, but the length of the constrained arc, where active thrusting is needed to contrast drag, is reduced, thus saving propellant. Drag
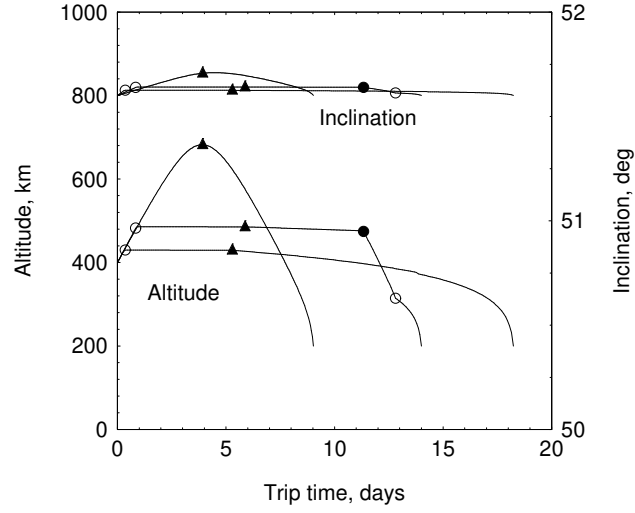
Figure 8: Minimum-propellant trajectories with dragsail for $\Delta a = -200$ km, $\Delta\Omega_0 = +10$ degrees (full circle = thruster on, empty circle = thruster off, full triangle = sail is opened) .
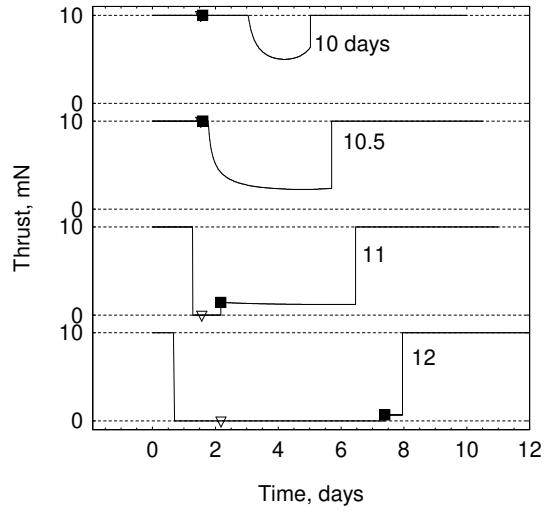

Figure 9: Thrust evolution for short minimum-propellant trajectories with dragsail for $\Delta a = +200$ km, $\Delta\Omega_0 = -10$ degrees (full square = start of constrained arc, empty triangle = sail is closed) .

only depends on altitude and is the same during the constrained arcs. Larger values of thrust (i.e., larger $\sin\beta$) when less time is available mean that more propulsive effort is dedicated to actively change the orbit plane.

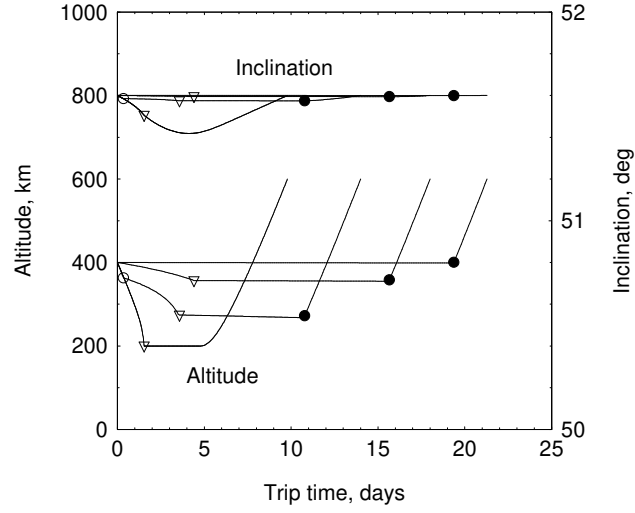At 12.5 days the minimum altitude is not reached: the sail is closed at a

24

Figure 10: Minimum-propellant trajectories with dragsail for $\Delta a = +200$ km, $\Delta \Omega_0 = -10$ degrees (full circle = thruster on, empty circle = thruster off, empty triangle = sail is closed)
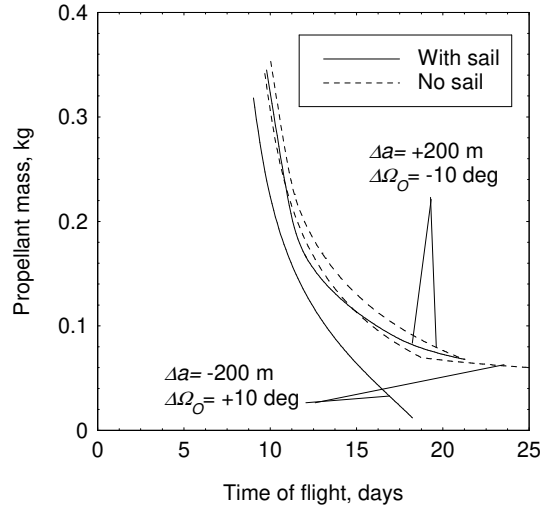.

Figure 11: Propellant consumption with dragsail for $\Delta a = \pm 200$ km, $\Delta \Omega_0 = \pm 10$ degrees.

proper altitude to wait for J2 to accomplish the desired plane rotation, before turning the thruster on and attain the final orbit. As shown in figure 10, which shows some trajectories for this case, at 14 days there is still a short initial propelled arc, whereas only the sail is used for altitude reduction at 18 days. The global optimum, at about 21 days, does not have the initial propelled/sail-

aided descent phase and only has the final thrusting arc. One should note that there is a slow altitude reduction during coasting arcs with sail closed, more visible at lower altitudes.

The benefit provided by the dragsail is shown in figure 11, which compares propellant consumption as a function of trip time for sail-aided transfers and solutions with no sail (the frontal area remains at the minimum value $0.04\mathrm{m}^2$), again for $\Delta a = -200$ km, $\Delta i = 0$, and $\Delta\Omega_0 = +10$ degrees, and $\Delta a = +200$ km, $\Delta i = 0$, and $\Delta\Omega_0 = -10$ degrees. The first case exhibits the larger improvements as the benefit of using the sail to reduce altitude is obvious: A one-day reduction of the minimum time can be attained, while the propellant reduction for the same time of flight ranges from about 80 g (shortest time) to about 60 g (in correspondence of the sail-assisted global optimum which only requires 12 g of propellant). Note that global optimum for the no-sail case is only attained at 58 days and has a 40 g propellant consumption.

Lower benefit is found for the case that requires an altitude increase, as expected. However, for the shortest time of flight, an initial height reduction is required to exploit J2, and the sail is still capable of providing propellant savings up to 30 g, whereas the benefit vanishes at the global optimum time (21 days, 68 g of propellant).

Table 6: Propellant consumption for $\Delta a = \pm 200$ km, $\Delta i = 0$ and $\Delta\Omega_0 = \pm 10$

	Trip time, days	Prop. consumption (with sail), kg	Prop. consumption (no sail), kg
$\Delta a = +200$ km $\Delta\Omega_0 = -10$	10	0.323	0.353 (min.time)
	15	0.113	0.130
	20	0.073	0.076
	21 (global opt.)	0.068	0.068
	Trip time, days	Prop. consumption (with sail), kg	Prop. consumption (no sail), kg
$\Delta a = -200$ km $\Delta\Omega_0 = +10$	9	0.318 (min. time)	-
	10	0.256	0.341 (min. time)
	15	0.064	0.113
	18	0.012 (global opt.)	0.075
	58	-	0.040 (global opt.)

Table 7 shows the CPU times that were required to obtain the first converged solutions for the transfers. All simulations where computed on an Intel(R) Core(TM) i7-4720HQ. The computational cost for the solution of the proposed problems results to be quite small. The authors did not encounter major problems with convergence when following the procedure described in Section 6. As for the maximum final mass problems, the times reported are the average of all transfers (from minimum time to global optimum). As a general

trend, problems that require the three-arc structure take the heaviest toll on CPU time, as expected. In addition, solution of scenarios without the dragsail tends to be faster.

Table 7: CPU time for minimum time and maximum final mass transfers

	Transfer	CPU time (ms)
Minimum time	$\Delta a = -200$ km, $\Delta i = 0$ and $\Delta \Omega_0 = +10$	322
	$\Delta a = -200$ km, $\Delta i = 0$ and $\Delta \Omega_0 = -10$	833
	$\Delta a = +200$ km, $\Delta i = 0$ and $\Delta \Omega_0 = +10$	293
	$\Delta a = +200$ km, $\Delta i = 0$ and $\Delta \Omega_0 = -10$	501
	Transfer	Avg CPU time (ms)
Maximum final mass	$\Delta a = -200$ km, $\Delta i = 0$ and $\Delta \Omega_0 = +10$	360 (with sail) 313 (no sail)
	$\Delta a = +200$ km, $\Delta i = 0$ and $\Delta \Omega_0 = -10$	489 (with sail) 284 (no sail)

8. Conclusions

Several mission concepts, such as active removal of multiple debris or servicing of satellite constellations, may require the evaluation of a large number of LEO transfers to define optimal strategies for the mission accomplishments (e.g., the removal/servicing sequence and the time length to be assigned to each mission leg). The indirect optimization approach proposed in this paper transforms the optimization problem into a boundary value problem with a limited number of parameters, which can be easily and rapidly solved. The proposed method therefore allows for fast evaluation of minimum-time and minimum-propellant transfers in LEO, thus enabling fast trade-off studies (e.g., trip time versus propellant) and preliminary analysis of problems involving large sets of targets. This method can be used as an alternative to existing techniques.

The analysis of several cases has highlighted the different strategies that may be optimal, depending on the transfer characteristics in terms of relative node position, orbital elements and available time of flight. Variations of semimajor axis and inclination are sought to change and exploit the effect of J2 on the orbit plane and limit the propellant consumption. The introduction of drag in the dynamical model allows for the analysis of trajectories aided with a dragsail. Relevant propellant savings can be obtained, in particular when an orbit height reduction is required, but also when the target orbit is higher and height reduction must be sought to increase J2 effect. These savings must be obviously contrasted to the weight of the sail system; for instance, if the $4 - \mathrm{m}^2$ sail provides a 100 g propellant saving, a specific weight below $25\mathrm{g/m}^2$ would make the sail convenient. The benefit of a dragsail obviously increases when multiple transfers are required, summing the propellant savings obtained with

the same dragsail in each transfer. There are hurdles to be solved before sail technological maturity becomes sufficiently high (for instance, related to drag deployment and retraction, possibly multiple times, and sail control) but these results seem promising.

References

[1] Fontdecaba Baig, J., Epenoy, R., Dargent, T., and Martinot, V., "A Method for Fast, Accurate and Robust Computation of Low-Thrust Transfers between LEO Orbits," 65th International Astronautical Congress (2014). Paper IAC-14-C1.8.2. doi:

[2] Di Carlo, M., Romero Martin, J.M., Vasile, M., "Automatic Trajectory Planning for Low-Thrust Active Removal Mission in Low-Earth Orbit," Advances in Space Research, 59, No. 5 (2017), 1234-1258. doi: j.asr.2016.11.033.

[3] Zuiani, F., Vasile, M., Avanzini, G., and Palmas, A., Direct Transcription of Low-Thrust Trajectories with Finite Trajectory Elements, Acta Astronautica, Vol. 72, 2012, pp, 108-120, j.actaastro.2011.09.011.

[4] Avanzini, G., Palmas, A., and Vellutini, E., Solution of Low-Thrust Lambert Problem with Perturbative Expansions of Equinoctial Elements, Journal of Guidance, Control and Dynamics, Vol. 38, No. 9, 2015, pp. 1585-1601, 10.2514/1.G001018

[5] Zuiani, F., Vasile, M., "Extended Analytical Formulas for the Perturbed Keplerian Motion under a Constant Control Acceleration," Celestial Mechanics and Dynamic Astronomy, 121, No. 3 (2015), 275-300. doi: 10.1007/s10569-014-9600-5.

[6] Yu, J., Chen, X.-Q., and Chen, L.-H., "Optimal planning of LEO active debris removal based on hybrid optimal control theory," Advances in Space Research, 55, No. 11 (2015), 2628-2640. doi: j.asr.2015.02.026.

[7] Olympio, J.T., and Frouvelle, N., "Space Debris Selection and Optimal Guidance for Removal in the SSO with Low-Thrust Propulsion," Acta Astronautica, 99 (2014), 263-275. doi: j.actaastro.2014.03.005.

[8] Graham, K. F., and Rao, A. V., "Minimum-Time Trajectory Optimization of Multiple Revolution Low-Thrust Earth-Orbit Transfers," Journal of Spacecraft and Rockets, 52, No. 3 (2015), 711-727. doi: 10.2514/1.A33187.

[9] Li, H., Chen, S., and Baoyin, H., "J2-Perturbed Multitarget Rendezvous Optimization with Low Thrust," Journal of Guidance, Control, and Dynamics, 41, No. 3 (2018), pp. 802-808. doi: 10.2514/1.G002889.

[10] Shen, H., and Casalino, L., "Full Access Simple ΔV Approximation for Optimization of Debris-to-Debris Transfers," Journal of Spacecraft and Rockets, 58, No. 2 (2020), 575-580. doi: 10.2514/1.A34831.

[11] Edelbaum, T. N., "Optimal Nonplanar Escape from Circular Orbits," AIAA Journal, 9, No. 12 (1971) 2432-2436. doi:10.2514/3.50047

[12] Cotten, B., Bennett, I, and Zee, R.E., "On-Orbit Results from the CanX-7 Drag Sail Deorbit Mission," 31st Annual AIAA/USU Conference on Small Satellites, AIAA (2017). Paper SSC17-X-06.

[13] Taylor, B., Underwood, C., Viquerat, A., Fellowes, S., Duke, R., Stewart, B., Aglietti, G., Bridges, C., Schenk, M., Massimiani, C., "Flight Results of the InflateSail Spacecraft and Future Applications of Drag Sails," 32nd Annual AIAA/USU Conference on Small Satellites, AIAA (2018). Paper SSC18-XI-04,

[14] Taylor, B., Fellowes, S., Viquerat, A., and Aglietti, G., "A Modular Drag-Deorbiting Sail for Large Satellites in Low Earth Orbit," AIAA Scitech 2020 Forum (2020). Paper AIAA 2020-2166. doi: 10.2514/6.2020-2166.

[15] Kechichian, J.A., "The Streamlined and Complete Set of the Nonsingular J2-Perturbed Dynamic and Adjoint Equations for Trajectory Optimization in Terms of Eccentric Longitude," The Journal of the Astronautical Sciences, 55, Nos. 3 (2007), 325-348. doi: 10.1017/9781108560061.013.

[16] Kechichian, J.A., "Optimal Low-Thrust Transfer in General Circular Orbit Using Analytic Averaging of the System Dynamics," The Journal of the Astronautical Sciences, 57, Nos. 1-2 (2009), 369-392. doi: 10.1007/BF03321509.

[17] Cerf, M., "Low-Thrust Transfer Between Circular Orbits Using Natural Precession," Journal of Guidance, Control, and Dynamics, 39, No. 10 (2016) 2232-2239. doi: 10.2514/1.G001331,

[18] Sidi, M.J., "Spacecraft Dynamics and Control," Cambridge University Press, Cambridge, 1997.

[19] Bate, R.R., Mueller, D.D., and White, J.E., "Fundamentals of Astrodynamics," Dover Publications Inc., New York, 1971.

[20] Cornelisse, J.W., Schöyer, H.F.R., and Wakker, K.F., *Rocket Propulsion and Spaceflight Dynamics*, Pitman, London, 1979.

[21] Bryson, A. E., and Ho, Y.-C., Applied Optimal Control, rev. ed., Hemisphere, Washington, DC, 1975, pp. 42-89.

[22] Casalino, L., Colasurdo, G., and Pastrone, D., "Optimal Low-Thrust Escape Trajectories Using Gravity Assist," Journal of Guidance, Control, and Dynamics, 22, No. 5 (1999) 637-642. doi: 10.2514/2.4451

[23] U.S. Committee on Extension of the Standard Atmosphere, U.S. Standard Atmosphere, 1976, U.S. Government Printing Office, Washington, DC, 1976.